FABRICATION AND TRANSPORT STUDIES OF N-TYPE OFETS USING ALIGNED ARRAY CARBON NANOTUBES ELECTRODES

by

EDWARDS G. JIMENEZ

A thesis submitted in partial fulfillment of the requirements
for the Honors in the Major Program in Electrical Engineering
in the College of Engineering and Computer Science
and in The Burnett Honors College
at the University of Central Florida
Orlando, Florida

Spring Term 2012

Thesis Chair: Dr. Saiful I. Khondaker

ABSTRACT

We present fabrication of n-type organic field effect transistors (OFETs) using densely aligned array carbon nanotube (CNT) electrodes. The CNTs were aligned with a high linear density via dielectrophoresis (DEP) from an aqueous solution. In order to fabricate the CNT electrodes, aligned CNTs were cut by using electron beam lithography (EBL) and precise oxygen plasma etching. The n-type OFETs were fabricated in a bottom-contact configuration by depositing a thin film of C60 molecules between the CNT source and drain electrodes, and compared against a controlled C60 OFET with gold electrodes. The electron transport measurements of the OFETs using CNT electrodes show better transistor characteristics compared to OFETs using gold electrodes due to improved charge injection from densely aligned and open-ended nanotube tips.

This thesis is dedicated to my mother and my father, who has supported my academic endeavors and encourages me to strive for excellence.

TABLE OF CONTENTS

LIST OF EQUATIONS

LIST OF FIGURES

CHAPTER 1: INTRODUCTION

1.1 Motivation

Organic field effect transistor (OFET) have attracted a lot of attention in the last decades due to low-cost fabrication and their application in transparent and flexible organic electronic devices [1-6]. Some of their applications vary from flexible, transparent displays, radio-frequency identification tags, and sensor arrays [Fig. 1-1]. OFETs are FETs where the active material is an organic semiconductor e.g. pentacene, Poly (3-hexylthiophene) P3HT, and Phenyl-C61-butyric acid methyl ester (PCBM) [7-9]. Up until now, OFETs were fabricated using metal electrodes such as gold and palladium, where the charge carrier injections are limited by the contacts of the electrodes/organic semiconductor interface [1, 3, 4].

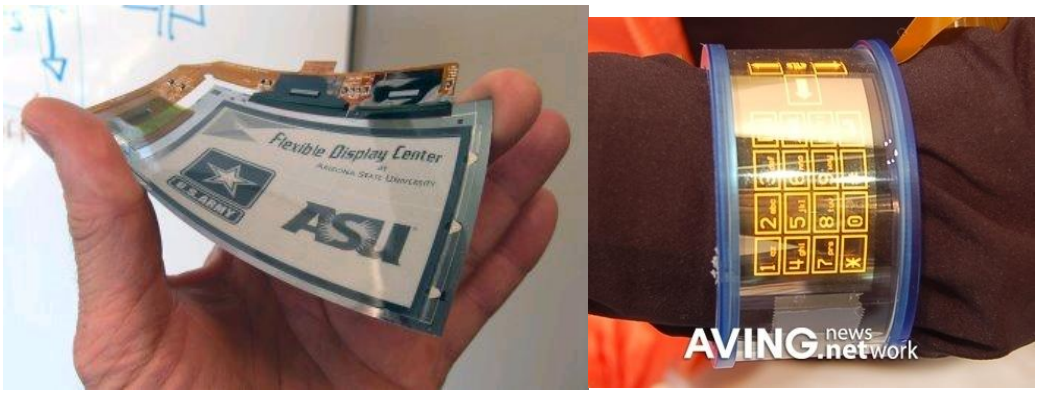

Figure 1-1: Flexible and transparent electronic devices. Ref. [10, 11]

The schematic diagram of the OFET is shown in Figure 1-2. As we can see from this figure that the charge transport in the OFET is limited by the two major factors. One is grain boundary of

the organic semiconductors (OSC) in the channel, and other one is interfacial barriers formed at the metal-OSC interface. When metal electrodes are contacted with OSC, different kinds of barriers are formed at the interface such as Schottky barrier, dipole barrier [3, 5, 12, 13]. In addition, these interfacial barriers are more dominating over the barrier formed by the grains boundaries of OSC in the short channel devices. The interfacial barriers shift the vacuum level of the semiconductor in comparison to the metal vacuum level [14]. As a result, the contact resistance between the metal and semiconductor becomes very large which limits the charge transport of the OFETs [3, 5]. Ideally, we want an ohmic contact, meaning that the contacts resistance is very small compared to the resistance of the OSC in the channel, which is unattainable by conventional metal electrodes [3, 5, 7, 14-16]. In this thesis, we focus on the charge injection from the electrode to OSC.

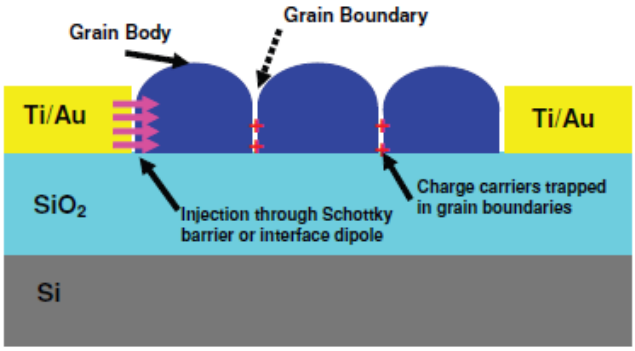

Figure 1-2: Schottky or Interface Dipole Barrier Ref. [17]

P-type OFETs are commonly fabricated with gold electrodes [1, 3, 4]. This is because work function of the gold matches with Highest Occupied Molecular Orbital (HOMO) level of most of p-type semiconductors and it forms a better contact than when used with p-type semiconductors. In comparison to p-type OFETs, fabricating an efficient n-type OFET we need to have an electrode with a work function that match the Lowest Unoccupied Molecular Orbital (LUMO) of the OSC. To

obtain the desired LUMO level, we need to use metals that have a low work function, such as calcium, magnesium, or aluminum instead of gold and platinum [4, 5, 18]. However, the problem in using low work function materials is that they get oxidized in contact with the atmosphere, which hinders electron transport [19, 20]. In addition, the contact resistance between metal electrode and an n-type OSC is much greater than the contact resistant between the metal electrode and the p-type OSC [15, 21]. This makes it more difficult to fabricate high performing n-type OFETs [22].

In order to overcome the limitations of the metal electrodes, carbon nanotube (CNT) having excellent electrical and physical properties, with one-dimensional nature and ballistic properties. CNT has been considered as a promising electrode material to overcome the limitations of metal electrodes for future electronic applications [2, 6, 23]. CNTs has been used as an active material in transistors, sensors, solar cells, or they act as interconnects of the transistor due to its high carrier density, highly conducting, flexible, and one-dimensional structure [2-4]. CNTs have been found to be an efficient charge injector because, at the nanotube apex, a large local field is generated when an electric field is applied [8, 24, 25]. But to fabricate large area electronic devices, a single CNT is not sufficient. Therefore, it is of great importance to develop a technique to attain an n-type OFET with high charge injection and mobility. In addition, CNTs offer the possibility of solution process, which will enable us to fabricate flexible and large area integrated circuits.

In this regard, recently our group have demonstrated the fabrication of the high performance p-type OFETs using array of aligned CNTs [9]. Shown in Figure 1-3, we observe a comparison of transistor performance of p-type pentacene with CNT and Au electrodes. The Pentacene/SWNT devices have a higher on-current and a bigger on/off ratio compared to the Pentacene/Gold device. From the box-plot shown in Figure 1-4, the maximum and average on-current for the

pentacene/SWNT devices are one order of magnitude higher when compared to pentacene/gold OFETs. Our group has also fabricated p-type OFETs by directly grown P3HT crystalline nanowires [8]. In both cases, compared to gold electrodes OFETs using CNT electrodes demonstrates enhanced charge injection, on current, on/off ratio, and mobility [8, 9].

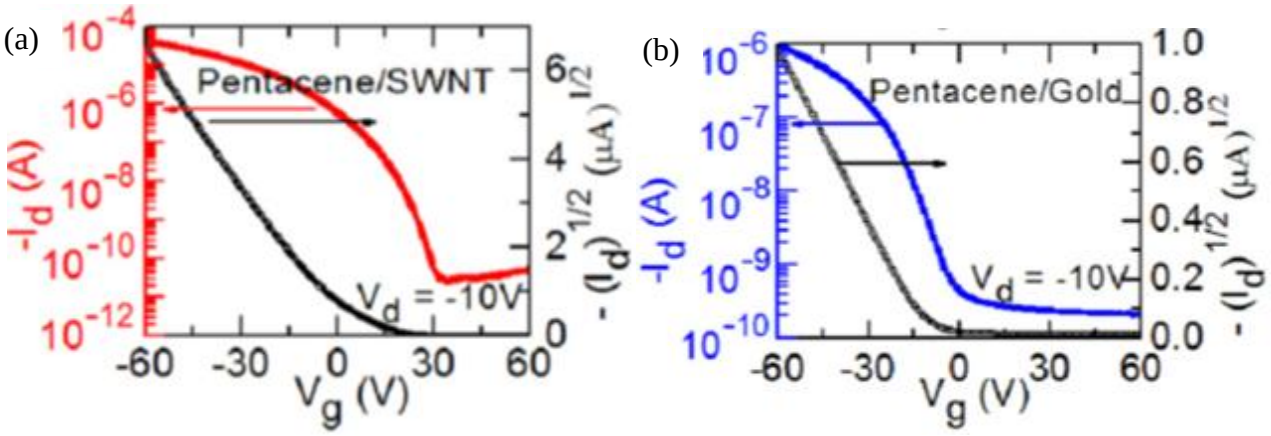

Figure 1-3: Transfer Characteristics (I_D versus V_G) at Vd=-10V for an OFET using (a) SWNT electrodes and (b) gold electrodes [9].

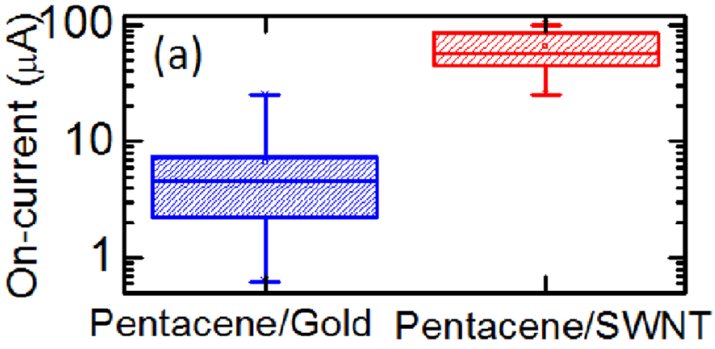

Figure 1-4: Box plot of the pentacene/SWNT and pentacene/gold on-current [9]

1.2 Organization of Thesis

In chapter two, I will discuss the limitations of using metal electrodes with an OSC in OFETs. In addition, I will provide the benefits of using carbon nanotubes as an electrode and a summary of several fabrication methods of implementing carbon nanotubes as an electrode.

Chapter three entails the fabrication techniques. Processes such as assembly of SWNT with DEP, electron beam lithography (EBL) to create electrodes, thermal deposition of the thin film, and the measurement setup will be described in details.

Next, in chapter four, the result of the OFETs fabrication and corresponding transport measurement will be discussed, such as the linear and saturation mobility, the on-current, the on/off ratio, and the threshold voltage. In addition, a comparison with our control device will be discussed regarding these parameters.

Finally, in chapter five, I will conclude with the impact of this results and future possibilities of this research.

CHAPTER 2: LITERATURE REVIEW

2.1 Organic field effect transistors

A typical OFET requires the following components: an OSC, which is separated from the gate electrode by the insulating gate dielectric layer, and the source and drain electrodes of a defined length and width that make contact with the semiconducting layer. In our fabrication we are implementing the bottom contact / bottom gate (BC/BG) configuration. Shown in Figure 2-1 is the BC/BG configuration with six parts. The first and second parts are the source and drain electrodes. The function of these electrodes are to insert and retrieve charge carriers to and from the OSC. The third part is the dielectric layer. This layer separates the gate from the OSC. In our device this part is made from silicon dioxide. The fourth part is the OSC. This part also known as the active material of the device, acts as an insulator until the required voltage is applied. Once the voltage reaches a certain threshold the device turns on. The fifth part is called the gate. We can control the current flowing between the source and the drain by varying the voltage applied between the source and the gate electrodes. The sixth part is the substrate. The substrate is the foundation for the device and is made of silicon.

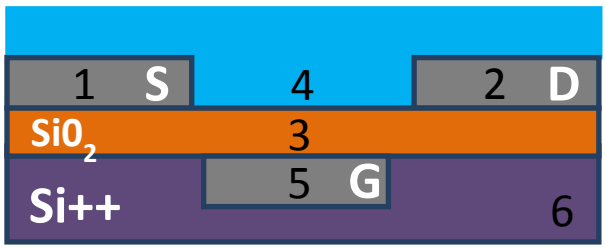

Figure 2-1: BC/BG OFET Configuration

An OFET operates when a voltage V_{DS} is applied between the source and drain, the source electrode is normally grounded. A positive gate voltage (V_G) will inject electrons from the source, the charge-injecting electrode, since the source electrode is always more negative than the gate electrode [5]. As soon as the threshold voltage (V_T) is applied on the gate of the transistor, current will start to flow between the drain and source. An inversion layer is created (See Figure 2-2A) between the source and drain, depending on the material. Depending on the charge of OSC a positive channel conducting holes or a negative channel conducting electrons will result.

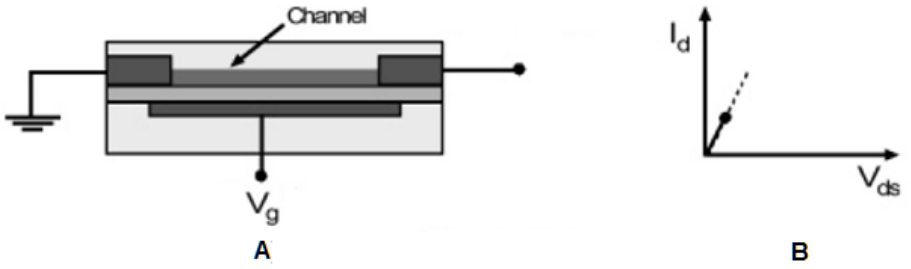

Figure 2-2: (a) Transistor channel across the two electrodes, (b) Graph shows the current in the linear region. Ref.[5]

When the OFET is in the linear region, shown in Figure 2-2B, the channel is still connected between the source and the drain electrode and no pinch off has occurred. In this region the current I_D flowing through the channel is directly proportional to V_{DS}. Increasing the voltage will increase the thickness of the channel resulting in an increase in the current flow until saturation is reached.

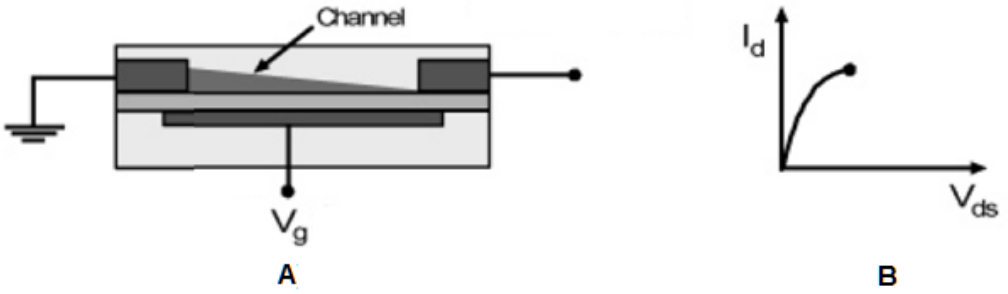

Figure 2-3: (a) Transistor reaching the start of saturation region, (b) Graph shows current started to reach saturation region. Ref. [5]

As the transistor is approaching the saturation regime the channel will slowly reach pinch off. Shown on Figure 2-3B, the current becomes constant as the voltage continues to increases. When saturation is reached, a pinched-off region is created that stops excessive current flow (See Figure 2-4A). That means a depletion region is formed next to the drain electrode, because the difference between the local potential and the gate voltage is now below the threshold voltage. In the saturation region, as the voltage is increased the depletion region moves towards the center of the channel, away from the source. While the depletion region goes deeper in the channel, the current barely increases, hence current becomes saturate.

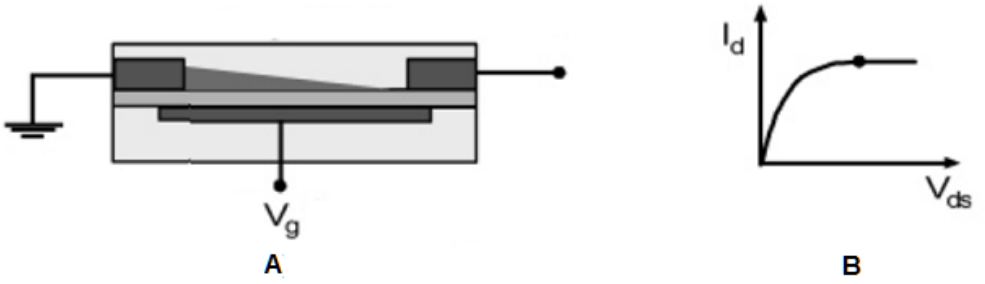

Figure 2-4: (a) Transistor showing pinch off, (b) Graph shows current in saturation. Ref. [5]

2.2 Metal electrodes and organic semiconductor interface

The OSC material is particularly important for the device performance, but the device performance is also extremely sensitive to the organic material-metal electrode interface [16, 23]. Various metals are used as electrodes in OFETs, but gold and palladium are more commonly used as source and drain electrodes for OFETs [13, 23, 24].

As mentioned before a Schottky and dipole barrier is formed at the interface that the metal electrode experience when contacted to the organic material [Figure 2-2]. Schottky barrier originates from a difference of energy level between the metal work-function and the HOMO (for hole injection) or the LUMO (for electron injection) of the OSC. This makes the metal-organic interfaces often non-Ohmic and the contact resistance very large and thus often limits the charge transport [12, 16, 24-26].

Dipole barrier on the other hand originate when there is a shift in the vacuum level of the material, this is depicted in Figure 2-2b [25]. When a metals vacuum level E_{VAC} (M) is different from the organic vacuum level E_{VAC} (O) a dipole barrier Δ is formed. An atomically clean gold electrode has a work function of ~5.2eV. But when this gold electrode comes in contact with an organic material, repulsion exists between the organic electron and the metal surface electron. This causes an electron tail compression followed by a decrease in the work function, known as push-back effect, and the work function drops to 4.5±0.1 eV, [13, 25]. This push-back effect gives the metal-organic interface an additional resistance, which in turn raises the contact resistance between the materials.

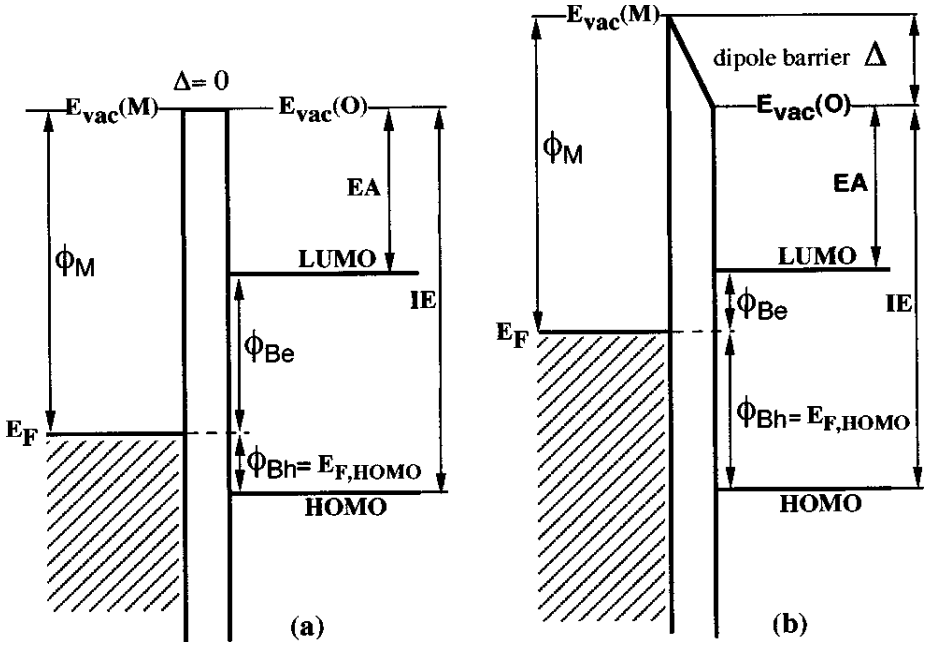

Figure 2-5: Organic-metal interface energy diagram (a) without and (b) with dipole barrier. Ref. [12]

Contact resistance has been shown to play a crucial role in transport characteristics [27-29]. Especially in short channel devices, where the channel is a few micrometers and below, contact resistance can easily dominate over the intrinsic channel resistance [28]. Another drawback of these metal electrodes is that they are not solution processed and they are not flexible. In addition to the flexible electrodes, solution processed electrodes can produce a less expensive electrode.

2.3 CNT electrodes as an alternate to metal electrode

Carbon nanotubes are made from rolling up graphene sheets [Fig 2-6]. Depending on the angle of the rolled up graphene sheet we can get semiconducting or metallic CNTs. For our research purposes we are using carbon nanotubes with metallic behaviors, these are made from rolling the graphene sheet. The CNT acts as a one-dimensional metal with a Fermi velocity that is comparable

to most metals [30]. With these ballistic, one-dimensional nature, high charge conductance we implement carbon nanotubes in our OFET.

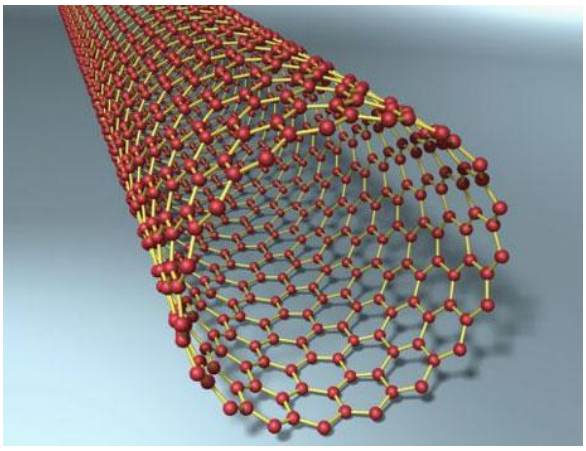

Figure 2-6: Carbon Nanotube Ref. [31]

It has been reported that in order to improve carrier transport an organic layer with an organic/organic layer interface has to be implemented [16]. In this regard, CNT has been considered as a promising electrode material to overcome the problem of dipole formation. One-dimensional (1D) structure of the CNT can optimize charge injection in OFETs, due to their strong field emission properties and π-π bonding at the electrode/semiconductor interface [7, 32, 33]. This field emission properties promote charge carrier tunneling across the Schottky barrier [9]. Besides the improvement in charge injection, there are several advantages to consider implementing CNT as an electrode. For example, π-π bonding, high electrical conductivity, compatibility in flexible electronics, and ease of processing [7, 34].

There have been different approaches reported for the fabrication of large area OFETs implementing CNT electrodes. Some common approaches are random network of CNT electrodes, CNT/polymer composite as an electrode material, anchoring CNTs using vacuum filtration method

[3, 7, 35-38]. All of these approaches have shown better performance compared to the control metal electrodes OFET devices.

To fabricate large area electronic devices, random network of CNT has been used to fabricate CNT electrodes [Fig. 2- 7a] [11, 39]. Since in this electrodes most of the CNT tips are randomly oriented and the channel length is not clearly defined, charge injection may occur from the base metal where the CNTs are anchored and also at the tips of these CNTs [10]. Another method of CNT electrode fabrication is by anchoring CNT electrodes onto a titanium contact using vacuum filtration method [Fig. 2-7b] [3, 7]. For this method, the alignment of the CNT appears to be random and the CNT density is very low, in addition since the dimension of the electrode is not well defined, charge injection may also occur from the titanium base electrode [35]. Alternative fabrication methods of CNT electrodes for OFET device have used CNT/polymer composite [Fig. 2-7c] [37]. One possible disadvantage of this method is that when applying a gate voltage to the OFET, it also modulates the electrodes which in turn affect the device performance [35].

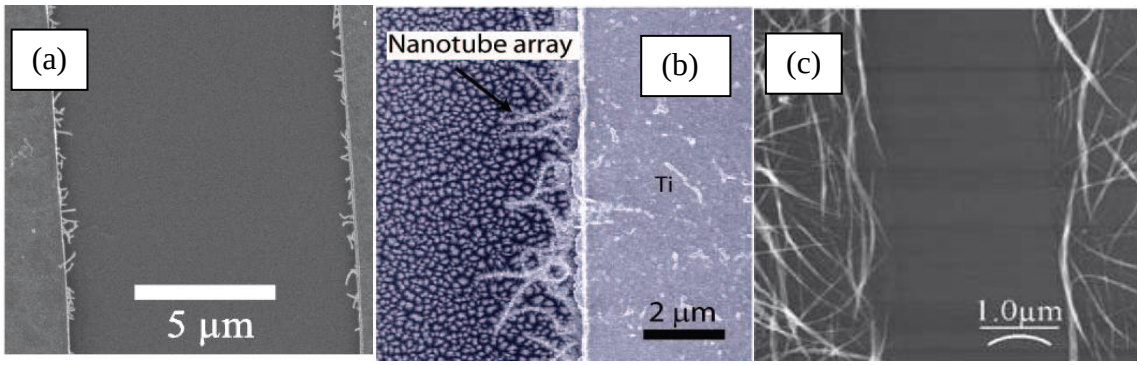

Figure 2-7: CNT electrodes using: (a) vacuum filtration method. Ref. [3], (b) Random network alignment. Ref. [7], (c) CNT/polymer composite. Ref. [37]

A solution to these problems is to use ultra-high density aligned CNT electrodes, where nanotube tips are parallel and channel length is well defined. Our group has fabricated ultra-high

density aligned array of CNTs with different densities [26]. As shown in figure 2-8a, we can observe a densely aligned CNT array with a density of 20 CNT/µm and in figure 2-8b a magnified image of figure 2-8a is shown. Our group also fabricated CNT arrays with a density of 30 CNT/ µm [Fig. 2-8c] a magnified image can be seen in figure 2-8d. Using these electrodes in our design will provide us with a well-defined channel length and tips that are parallel to one another [35].

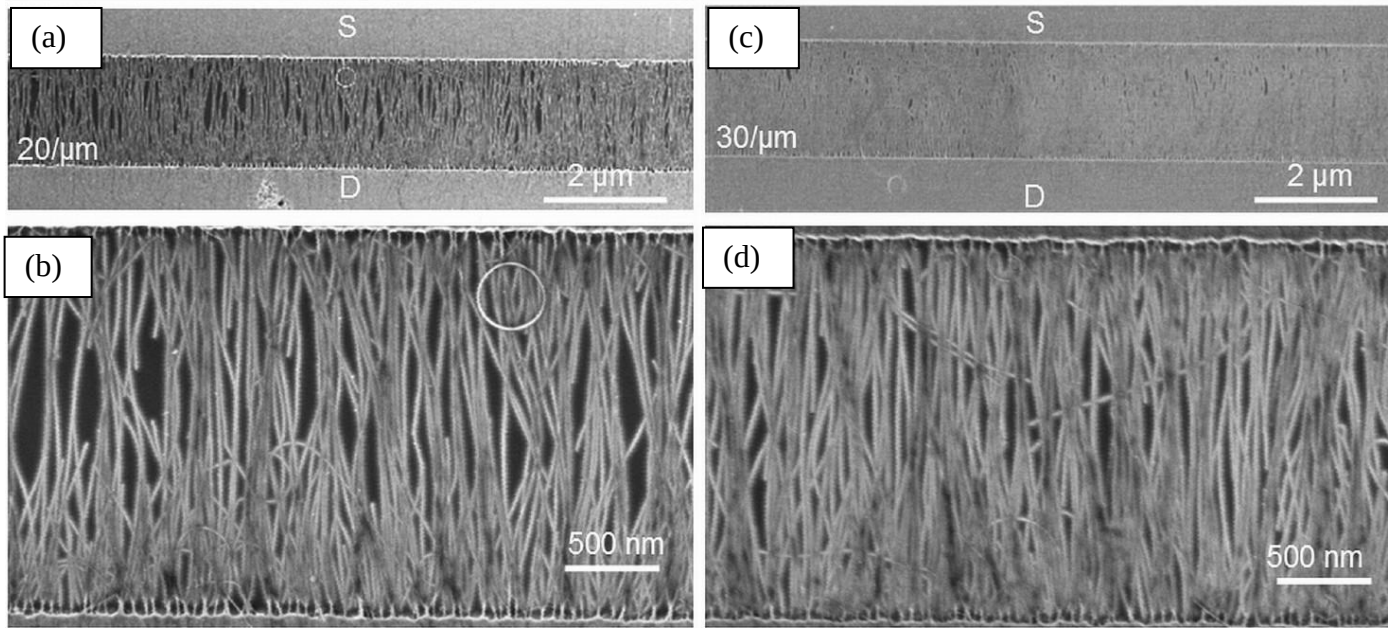

Figure 2-8: Scanning Electron Microscope (SEM) image of ultra-high density aligned CNTs with (a) a density of 20SWNT/µm and (b) 30SWNT/µm, (c, d) Magnified image of (a) and (b). Ref. [26]

CHAPTER 3: DEVICE FABRICATION AND EXPERIMENTAL METHODS

We used silicon wafer as substrate which is capped with a thermally grown 250 nm SiO_2 layer. We fabricated large contact pads, electron beam lithography (EBL) markers, as shown in Figure 3-1a, using photolithography. In order to perform EBL, PMMA is spin-coated onto the wafer at 4000 rpm for 1 minute, afterwards baked on a hot plate for 15 minutes at 180^{o}C. After EBL, the sample is developed in methyl isobutyl ketone (MIBK) and isopropanol (IPA) mixed at 1:3 ratio for ~70 s. After a final rinse in IPA for ~10 s the sample is blown dry with nitrogen gas.

After that EBL was used to define patterns of 5 µm x 25 µm to anchor the CNT and followed by thermal evaporation of 5 nm Chromium (Cr) and 30 nm palladium (Pd). In order to remove excess metal, the chip is placed in an acetone at 60^{o}C for ~15 minutes. After all the surplus metal has been removed, we clean the substrate with acetone, isopropanol and deionized water. To dry the substrate, we blow the deionized water off with a stream of nitrogen gas. There are nine electrode pairs on each design as shown in Figure 3-1b. An exploded view can be seen in Figure 3-1c.

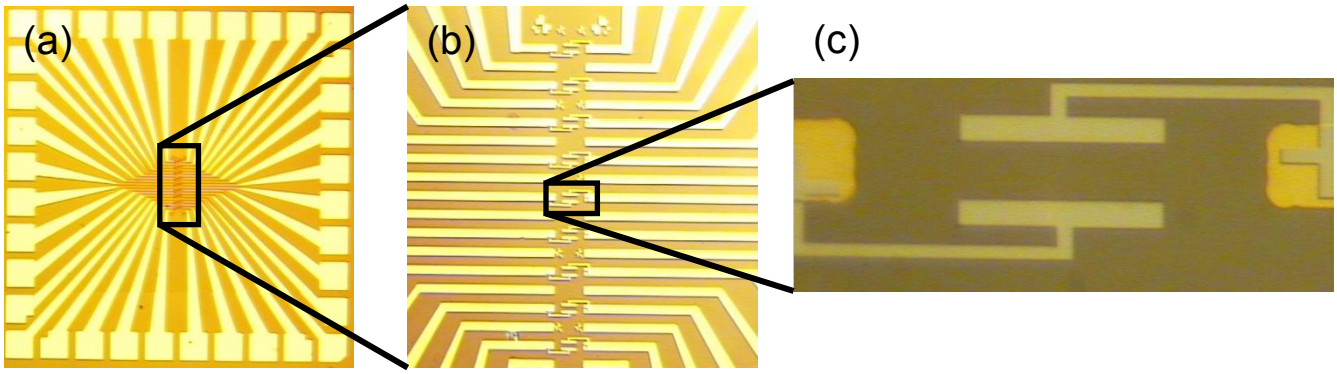

Figure 3-1: Typical micro electrode for device assembly. (a) Optical image of the chip with nine gold patterned electrodes. (b) Expanded optical image of the 9 electrode pairs. (c) Expanded image of a single electrode pair with a channel length of 5 µm.

3.1 Assembly of CNT by Dielectrophoresis

We aligned CNTs in a dense array between the Pd patterns *via* dielectrophoresis (DEP) [Figure 3-3a]. Aqueous solution of CNT was obtained from Brewer Science and was diluted by three times in DI water. In figure 3-2 we can see the CNT length and diameter distribution in the solution. The average CNT length is ~1.5 µm and the average diameter is ~1.7 nm. For DEP, a 3 µL drop of the solution with a density of 17 µg/mL was placed on the Pd pattern and an AC voltage of 5Vpp at 300 kHz was applied for 45 seconds. Due to DEP force, SWNT are aligned between the Pd patterns. The cartoon of the assembled CNT between prefabricated Pd patterns can be seen in Figure 3-3c.

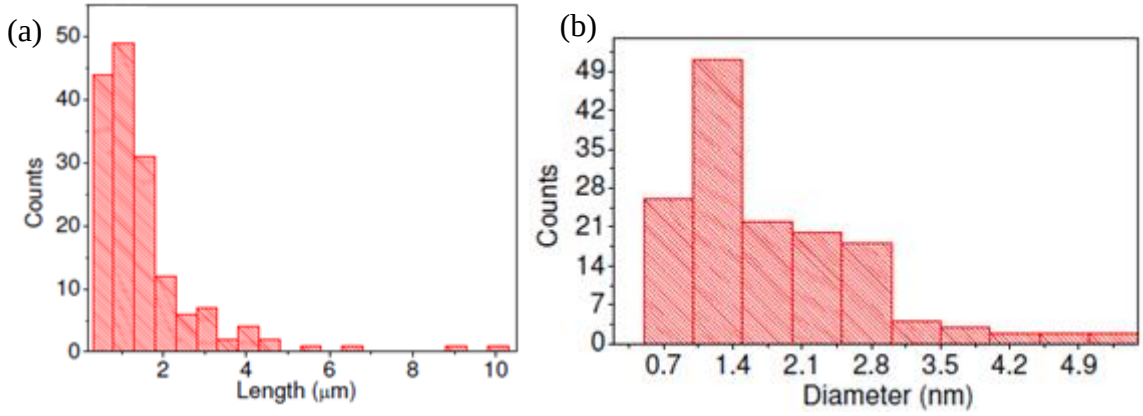

Figure 3-2: (a) Length distribution of nanotubes with an average length of ~1.5 µm, (b) Diameter distribution of the CNTs in the solution with an average height of ~1.7 nm. Ref. [26]

When applying an AC-voltage, the voltage gives rise to a time averaged DEP force (F_{DEP}) between the Pd patterns and aligns the CNTs, which is given by the following formula [40]:

$$F_{DEP} \infty \mathrm{Re}[\frac{\varepsilon_p - \varepsilon_m}{\varepsilon_p + 2\varepsilon_m}]\nabla|E|^2 \quad (1)$$

Where E = Electric field, ε_m= complex permeability of the medium, ε_p = complex permeability of the particle. By applying an AC voltage we can induce a dipole moment on the CNT [19]. In Figure 3-3b, one can see that when AC voltage is applied, a strong electric field is induced between the Pd patterns. This will cause the CNTs to move to the area with the strongest electric field and align uniformly between the Pd patterned.

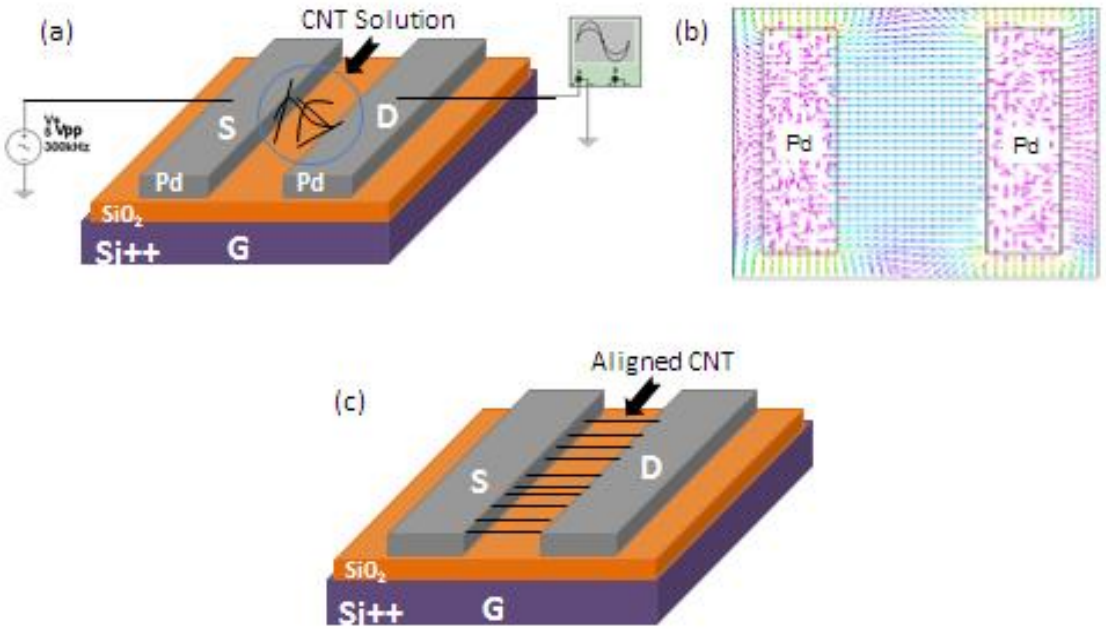

Figure 3-3: Alignment of SWNT electrodes. (a) CNT solution being dropped between the Pd electrodes and DEP is performed, (b) When the induced dipole moment of the carbon nanotube interacts with strong electric field, this causes the carbon nanotubes to move uniformly along the electric field gradient and align between the source/drain electrodes, (c) Aligned SWNT electrodes.

3.2 CNT electrode fabrication

After the CNT assembly, we deposited the PMMA solution on top of the chip and spin-coated at 4000 rpm for 60s followed by baking for 15 min at 180^{o}C on a hot plate [Figure 3-4a]. The CNT patterns of channel length L=2 μm and width W= 25 μm were defined by EBL writing and later developed in methyl isobutyl ketone (MIBK) and isopropanol (IPA) mixed at 1:3 ratio [Figure 3-4b]. The samples were placed into an oxygen plasma chamber for 10 min and exposed CNTs were etched away through the open window [Figure 3-4c]. Finally the CNTs were kept in chloroform for twelve hours and rinsed with acetone, isopropanol, and deionized water respectively to remove the PMMA [Figure 3-4d]. The surface can then be dried using nitrogen gas. Gold electrodes with the same geometry as our CNT electrodes were fabricated for control experiments by EBL followed by thermal deposition of gold and standard lift off.

To verify the CNTs alignments, we took scanning electron microscope (SEM) images using Zeiss Ultra – 55 SEM with an accelerating voltage of 1 kV. Once the CNTs were aligned, measurements were taken to obtain the electrical properties of the assembled CNTs. Electrical transport measurements of the CNTs array were performed by DL instruments 1211 current amplifier and a Keithley 2400 source meter interfaced with LabView program. By applying a DC voltage of -50 to 50 mV across the electrodes showed us the SWNTs electrical properties. With the use of the program LabView we calculated the resistance of the SWNT electrodes.

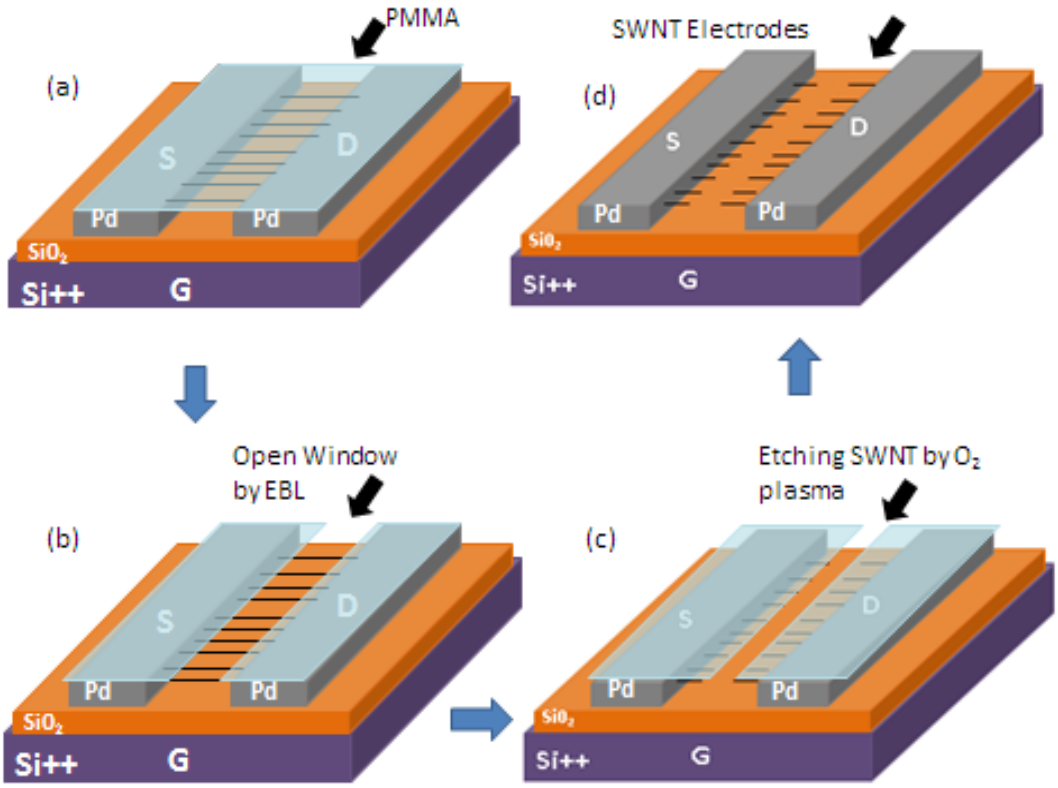

Figure 3-4: Fabrication schematic of SWNT electrodes. (a) PMMA resist is spin coated, (b) Open a window with EBL, (c) Exposed SWNTs are etched by oxygen plasma, (d) SWNT electrodes after removing PMMA with chloroform.

Figure 3-5a shows a representative SEM image of the aligned array CNT via DEP between the palladium electrodes. A high magnification SEM image of this array is shown in the inset. Figure 3-5b shows a SEM image of our fabricated CNT electrodes with a well-defined channel length and width. The measurement diagram shown in Figure 3-5c, is the measurement setup we used to measure the IV-curves. Current voltage characteristics of the aligned arrays are shown in Figure 3-5d and calculated resistance of this array is 600 ohm. To confirm, no nanotube tube remained in the

CNT electrode channel, we also measure IV of the electrode and we found a negligible current flow between the electrodes.

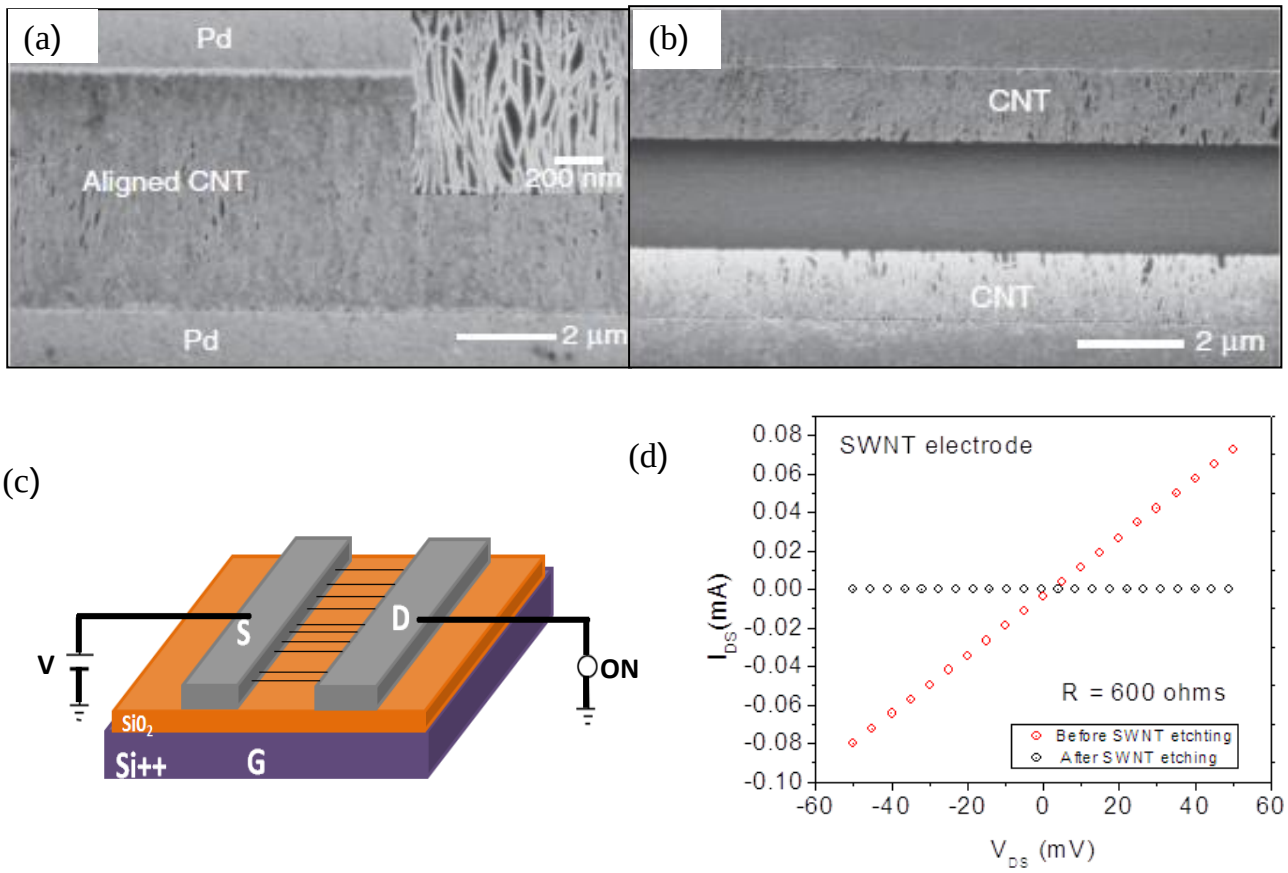

Figure 3-5: (a) SEM image of aligned SWNT electrodes inset shows magnified images of CNT [20], (b) CNT electrodes after cutting, (c) CNT Measurement Schematic, (d) Drain current as a function of bias voltage with no gate voltage applied .

In the histogram of Figure 3-6, we measured the resistance of 28 electrodes of the aligned CNTs, we got on average around 650 Ω with a corresponding sheet resistance of 3.25 KΩ/sq. The low resistance and sheet resistance makes these CNT arrays an ideal candidate for OFET electrodes.

Sheet resistance (R_S) can be calculated with the following formula:

$$R_S = \frac{W}{L} * R \qquad (2)$$

Where R = CNT electrode resistance, W = channel width, and L = channel length.

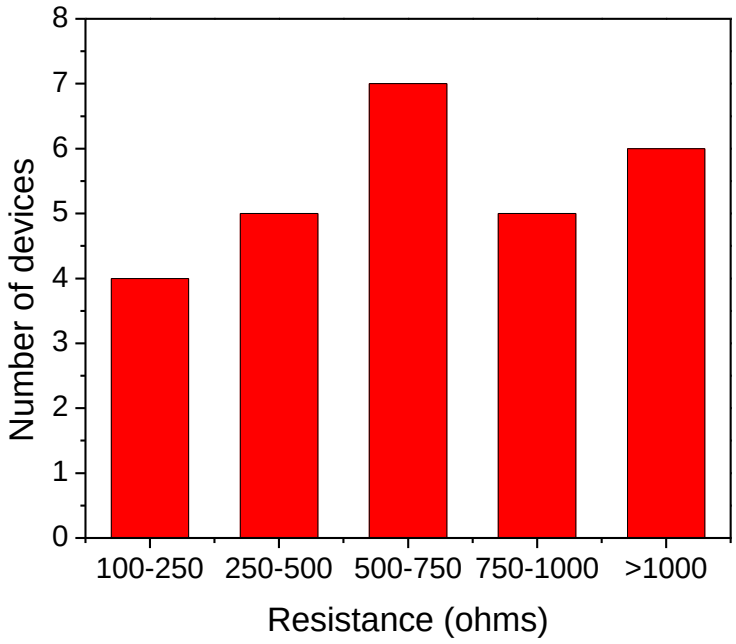

Figure 3-6: Histogram of the resistance values of the aligned M-SWNT electrodes.

3.3 Thermal deposition of C60

Once the electrodes are fabricated, the next step is to deposit an organic semiconductor layer on top the electrodes. The semiconducting material that we deposit is called buckminsterfullerene also known as Buckyball (C60) [Figure 3-7c], this is an n-type material. First we placed chips containing the CNT and gold electrodes in the thermal chamber and then we insert the C60 powder in the crucible. The thermal chamber is locked and pumped down to about 1 x 10^{-7} mbar, this takes ~25 minutes. Once the desired pressure is reached the thermal evaporation begins. We deposited a 30 nm

layer thick of C60 with deposition rate of ~ 0.15 Å/s. C60. The atomic force microscopy (AFM) image of the C60 layer is shown in Figure 3-7. AFM images were acquired using tapping mode atomic force microscopy (AFM) by Dimension 3100 AFM (Veeco). By analysis of the AFM images we found that the grain size of the C60 is ~ 50 nm with rms value of the surface roughness of ~ 2.5 nm.

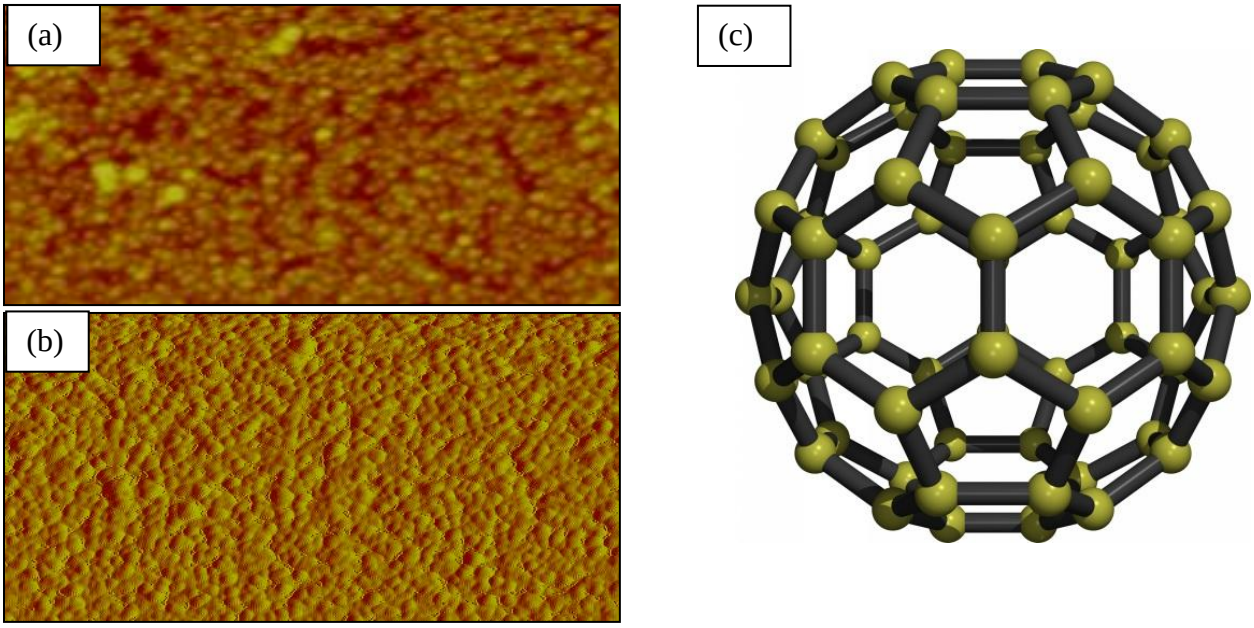

Figure 3-7: AFM images of a deposited C60 thin film, (a) height AFM image, (b) amplitude AFM image, (c) C60 molecule structure Ref. [41].

3.4 Measurement setup for OFETs

All of the fabricated devices have the same geometry of L = 2µm and W=25µm. With Hewlett-Packard (HP) 4145B semiconductor parametric analyzer connected to a probe station inside a nitrogen-gas glove box, we measured room temperature OFET transfer and output characteristics. The measurement schematic is shown in Figure 3-8. To measure the transfer characteristics we applied a voltage of -80 to 80V at the gate electrode (V_G) and applied a drain to source voltage of

20V (V_{DS}). For the output characteristics we applied a drain voltage (V_D) from 0 to 80V and a gate voltage (V_G) from 40 to 80V.

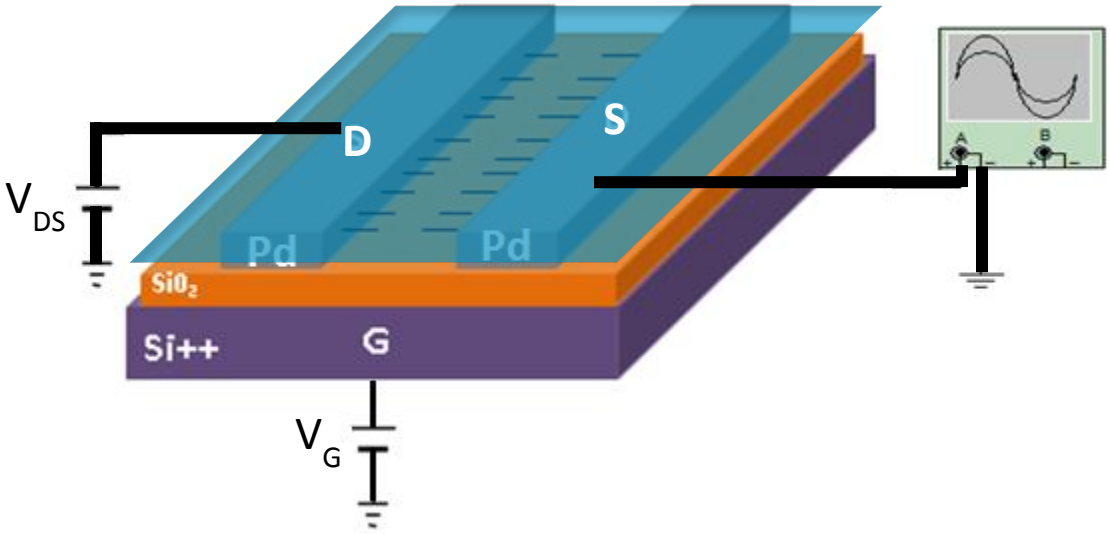

Figure 3-8: OFET measurement Schematic

CHAPTER 4: ELECTRON TRANSPORT MEASUREMENT OF C60 OFET

4.1 Introduction

By analysis of the OFET output and transfer characteristics we can find its on/off ratio, linear and saturation mobility, threshold voltage, and on-current. The on-off ratio is calculated by measuring at what current level the transistor turns on and at what current level it turns off. The on and the off current are controlled by different factors of the device. The on current is controlled mainly by the mobility of the semiconductor and the capacitance of the gate dielectric. Nonetheless, the off current is determined by the gate leakage and the unintentional doping of the semiconductor [5]. The on-off ratio should be as large as possible. This ensures a clean switching behavior between the on and off state of the transistor. Another parameter that we can measure from transfer characteristics is the device mobility. The mobility of the transistor depends on the electrode and the OSC you use in the manufacturing of your OFET. Mobility describes the ease with which electrons or holes drifts through the material. Depending on the material, different charged drifts will occur. If the material is negative (n-type), then electron drift takes place; or, if the material is positive (p-type), hole drift takes place when current is passed through the material.

The faster an electron or hole drifts through the material the higher the mobility will be. The linear mobility is an important parameter to observe the contact barrier of an OFET because the linear region of the output characteristics of the OFETs is related to the contact.

We can calculate the linear mobility with the equation shown below:

$$\mu = \frac{\left(\frac{dI_d}{dV_g}\right) * L}{W * C_i * V_d} \quad (3)$$

Where L = channel length, W = channel width, V_D = drain voltage, C_i = capacitance per unit area of the gate insulator.

We also analyzed the saturation mobility of our devices using following equation:

$$\mu = \frac{I_D * 2L}{W * C_i * (V_G - V_T)^2} \quad (4)$$

Where I_D= drain voltage, L = channel length, W = channel width, C_i = capacitance per unit area of the gate insulator, V_G = gate voltage, V_T = threshold voltage.

4.2 OFET transfer and output characteristics

We fabricated 15 devices using CNT electrodes and 15 devices using gold electrodes as our control devices.

4.2.1 CNT electrodes OFET

The measured output characteristic of the best CNT/C60 device is shown in Figure 4-1a. This device shows excellent gate modulation of the output current and also current saturation.

The electronic transfer characteristics ($I_{DS} - V_G$) for the same CNT/C60 device at a fixed V_{DS} = 20 V is shown in Figure 4-1b. From this Figure we can observe that the current varies over four

orders of magnitude (I_{on}/I_{off} = 2 x 10^4) to a maximum current of 2x10^{-5} A at V_G =80V. The device shown in Figure 4-1 had a threshold voltage (V_T) of 10V. We will show in section 4.2.3 how the threshold voltage is measured. From equation 3 we can calculate the standard linear mobility of this particular device. Where L = 2µm, W = 25 µm, V_D = 20V, C_i = 13.8 nF/cm^2. The linear mobility for the best device that we calculated was 0.116 cm^2 / V·s. From equation 4 we can calculate the saturation mobility of this particular device. We calculated saturation mobility of our device and found to be 0.042 cm^2 / V·s.

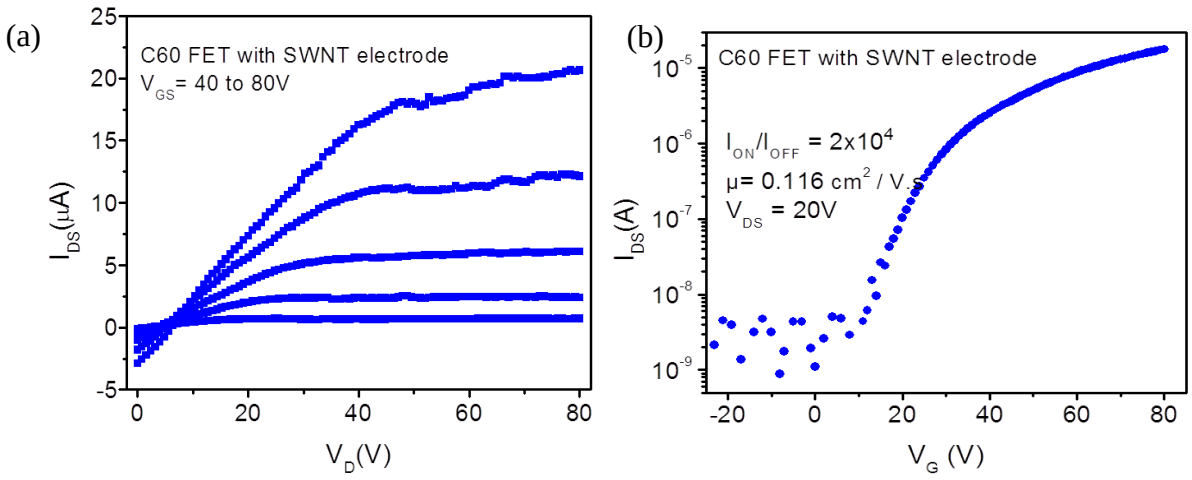

Figure 4-1: (a) Output characteristics of C60 OFET for L=2 µm and W =25 µm with SWNT electrode. (b) Transfer characteristics at fixed VD = -20 V of CNT/OFET devices.

4.2.2 Gold electrodes OFET

The output characteristic of the best Gold/C60 device is shown in Figure 4-2a. This devices shows a lower saturation current of 10 µA (at V_G = 80V and V_D = 80V) compared to the CNT/C60 device.

The transfer characteristics ($I_{DS} - V_G$) for the same Gold/C60 device at a fixed V_{DS} = 20V is shown in Figure 4-2b. From this figure we can observe that the current varies over four orders of magnitude (I_{on}/I_{off} = 4 x 10^4) to a maximum current of 4x10^{-5} A at a V_G = 80V. The device shown in Figure 4-2 had a threshold voltage (V_T) of 40V. From the equation 3 we calculated the linear mobility of this particular device. Where L, W, V_D, and C_i have the same values of L=2µm, W=25µm, Vd=20V, and Ci = 13.8 nF/cm^2. The linear mobility that we calculated was 0.055 cm^2 / V·s. From the equation 4 we calculated the saturation mobility of this particular device. For our saturation mobility we calculated a value of 0.089 cm^2 / V·s.

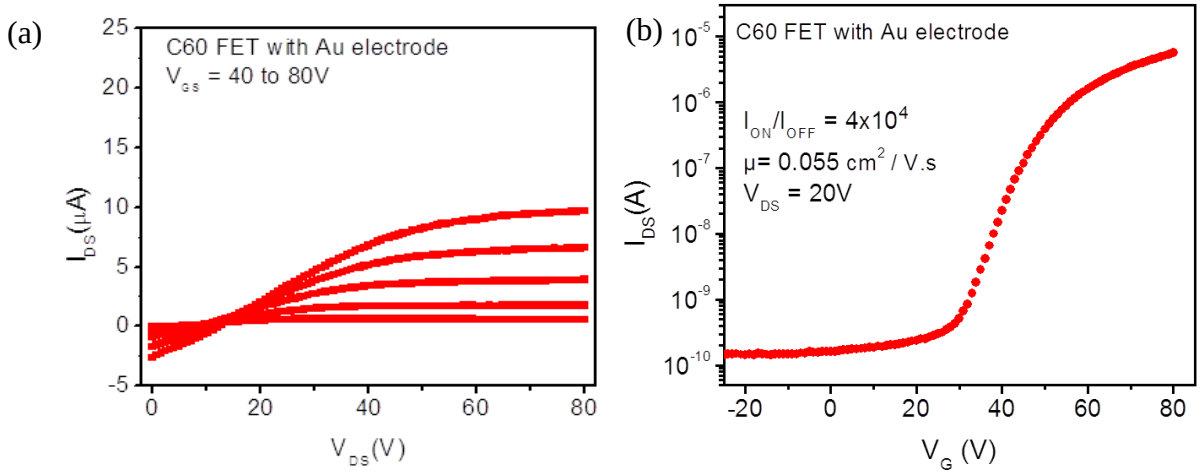

Figure 4-2: (a) Output characteristics of C60 OFET for L=2 µm and W =25 µm with Au electrode. (b) Transfer characteristics at fixed VD = -20 V of Au/OFET devices.

4.2.3 OFET devices performance comparison

Out of 15 CNT electrode OFETs and 15 gold electrode OFETs we measured, we found the average and maximum transfer and output characteristics of the deposit C60 thin film in combination with CNT and gold electrode devices. We measured 15 CNT/C60 devices, and we found a linear

mobility of these devices is in the range of 0.04 – 0.182 cm^2 / V·s with an average of 0.086 cm^2 / V·s. For the control devices, the linear mobility for the Gold/C60 devices is in the range of 0.001 – 0.058 cm^2 / V·s, showing an average of 0.024 cm^2 / V·s. In Figure 4-3 we can observe that Gold/C60 OFETs have a broader range, thus the CNT/C60 OFETs show a more uniform behavior. From table 1 we can observe that CNT electrode OFETs has a maximum and average linear mobility ~3 times higher in comparison to gold electrodes OFETs.

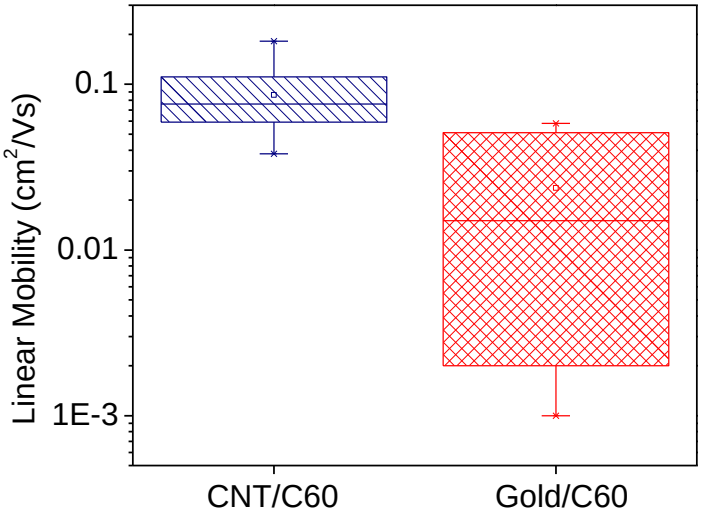

Figure 4-3: Linear Mobility boxplot of CNT/C60 and Gold/C60 OFETs

Saturation mobility is another important parameter that provides the overall device performance. For our CNT/C60 OFETs we measured a maximum saturation mobility of 0.16 cm^2 / V·s with an average of 0.07 cm^2 / V·s. The range of saturation mobility calculated is 0.02 - 0.16 cm^2 / V·s. In comparison for our control devices fabricated from Gold/C60 we calculated a maximum saturation mobility of 0.09 cm^2 / V·s with an average of 0.03 cm^2 / V·s. The range of saturation

mobility for our Gold/C60 devices calculated is 0.003 - 0.09 cm^2 / V·s. From these measurements we can observe that CNT/C60 devices have a maximum and average saturation mobility of ~2 times higher in comparison to our control Gold/C60 OFETs. Thus CNT/C60 OFETs shows a better overall performance in comparison to Gold/C60 OFETs. Looking at Figure 4-4, the CNT/C60 OFETs shows a more uniform behavior in comparison to the Gold/C60 OFETs. The Gold/C60 OFETs show a broader range of saturation mobility in comparison to the CNT/C60 OFETs.

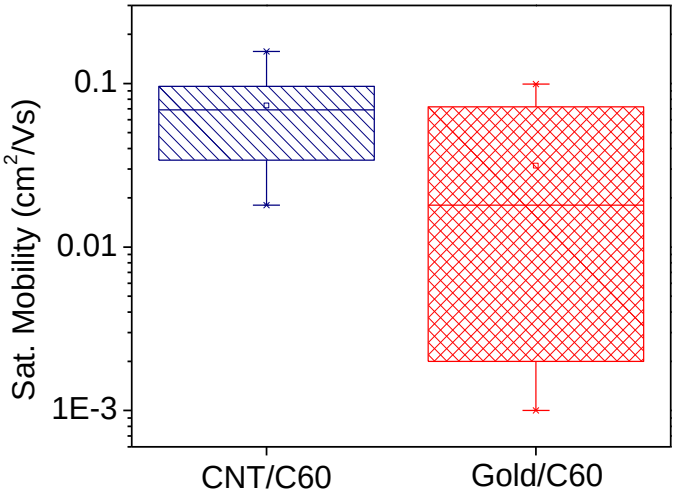

Figure 4-4: Saturation Mobility boxplot of CNT/C60 and Gold/C60 OFETs

When analyzing the electron transport characteristics we obtained a higher on-current in the CNT electrodes OFETs compared to the control gold electrode OFETs. From the boxplot shown in From the Figure 4-4, we can see that the maximum and average on-current of the 15 CNT/C60 devices are higher than that of the gold/C60 devices. To calculate the on-current we measure the current from the transfer characteristics at V_G=80V and V_{DS}=20V. For the on current in the CNT/C60 devices, we got a maximum and average of 18 µA and 9.6 µA, respectively. In comparison our control Gold/C60 devices got an on current maximum and average of 5.6 µA and

2.1 µA. Accordingly, both the maximum and average are ~3 times higher for the CNT/C60 OFETs compared to the control Gold/C60 OFETs. In Figure 4-5, we can also observe the uniform behavior of the CNT/C60 electrodes compared to the Gold/C60 electrodes. Again the Gold/C60 OFETs shows a broader range of on-current. Therefore CNT/C60 OFETs are fabricated more uniform.

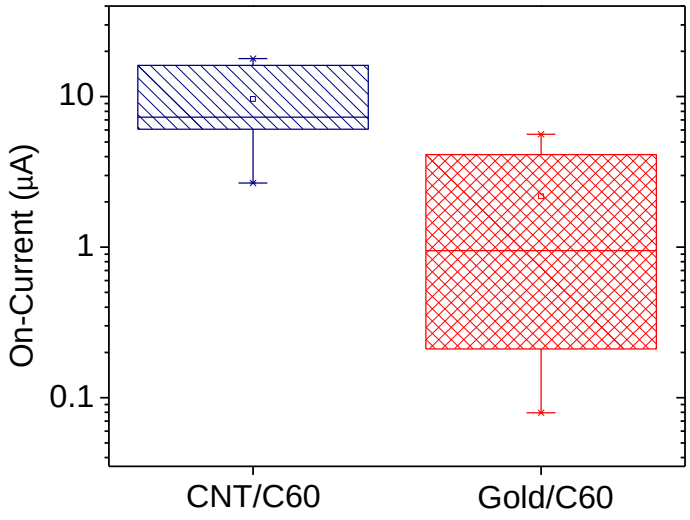

Figure 4-5: On-Current boxplot of CNT/C60 and Gold/C60 OFETs

Another parameter that was measured was the current on/off ratio, shown in Figure 4-6. For the CNT/C60 OFETs we obtained a maximum and average on/off ratio of $1.5x10^5$ and $6.1x10^4$, respectively. The range of the CNT/C60 OFETs on/off ratio was from $1.4x10^4$ to $1.5x10^5$. For the control Gold/C60 devices we measured a maximum and average on/off ratio of $3.4x10^4$ and $1.3x10^4$, respectively. The on/off ratio range for the control Gold/C60 OFETs was from $2.5x10^2$ to $3.4x10^4$. Thus the maximum and average current on/off ratio reported for the CNT/C60 OFET is ~4 times higher than the reported value of our control Gold/C60 OFET. The higher results reported for the

CNT/C60 OFETs shows a well modulation of drain current when a gate voltage is applied. In Figure 4-6 the CNT/C60 OFETs shows a more uniform behavior when compared to the Gold/C60 OFETs.

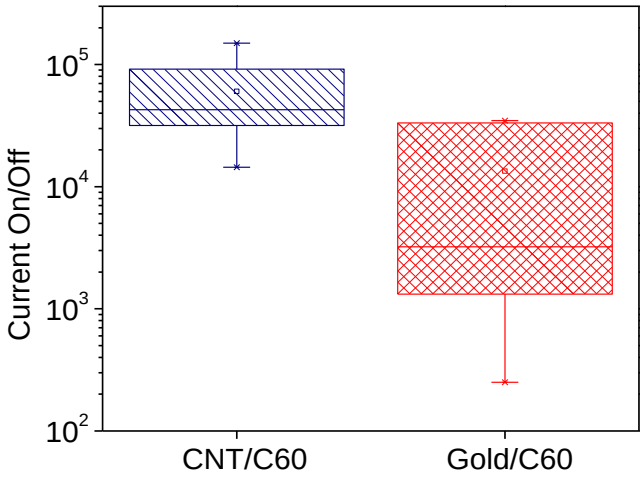

Figure 4-6: Boxplot of CNT/C60 and Gold/C60 OFETs current On/Off ratio

The last parameter that was measured was the threshold voltage. We measured the threshold voltage by plotting the transfer characteristics ($I_D - V_G$) curve in the linear region. By extrapolating from the point where V_G = 80V towards the point where the OFET is off, we find where the extrapolated line crosses zero, at this point is the threshold voltage [Figure 4-7a]. For CNT/C60 OFETs we measured a minimum and average threshold voltage of 10V and 21V, respectively [Figure 4-7b]. Compared to our CNT/C60 devices, for our control devices of Gold/C60 we got a minimum and average value for the threshold voltage of 30V and 36V, respectively. An increase in the threshold voltage means the presence of a larger injection barrier [42]. Therefore the Gold/C60 OFETs have a larger injection barrier compared to our CNT/C60 OFETs.

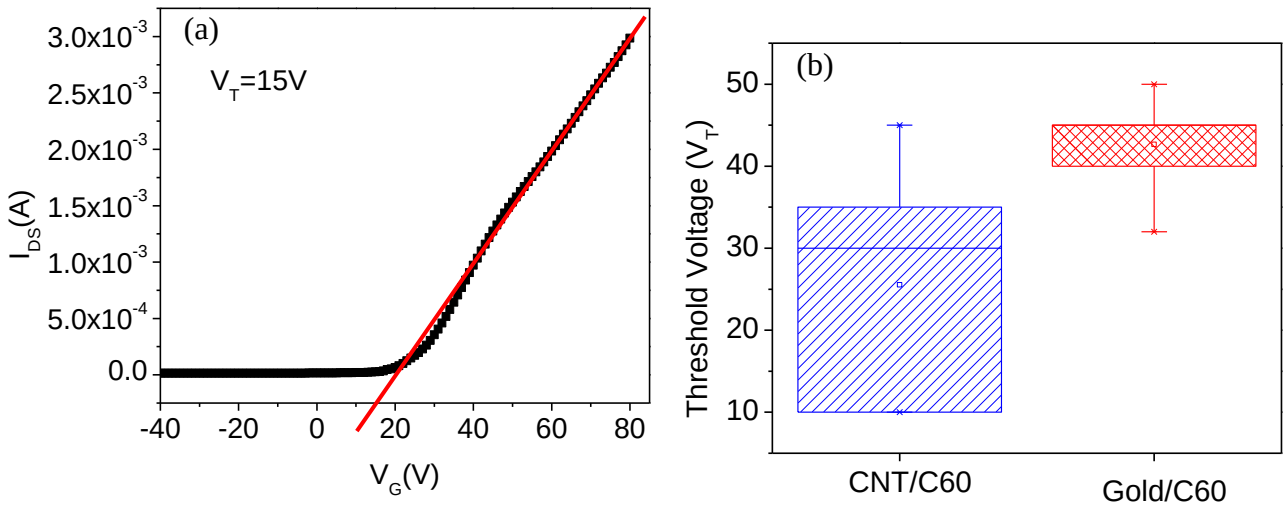

Figure 4-7: (a) calculating the threshold voltage by extrapolating, (b) threshold voltage boxplot of CNT/C60 and Gold/C60 OFETs

This lower threshold voltage and higher on-current in CNT OFETs shows that there is a better charge injection from CNT compared to gold due to the strong π-π interaction between the CNT and the organic material interface. Another attribute that leads to a better charge injection for the CNT electrodes are the electric field emission from the nanotube tips, due to the one-dimensional property that the CNTs possess. These field emissions are enhanced by having the nanotubes ends open-ended [43]. Consequently, combining the use of ultra-high density (~20-25 CNT/μm) parallel CNT electrodes with the synchronized field emission of these open-ended CNT electrodes leads to a higher charge injection.

From Table 1 we can see an overview of all the measured parameters for CNT/C60 and Gold/C60 OFETs. CNT/C60 OFETs had higher value for linear and saturation mobility, on-current, on/off ratio, and a lower threshold voltage in comparison to the control Gold/C60 OFETs. All these values points out a better performance for the CNT/C60 OFETs, due to a smaller barrier between the CNT electrode and the C60.

OFET	CNT/C60	Gold/C60
Linear μ (cm^2 / V·s) (max.)	0.18	0.06
Linear μ (cm^2 / V·s) (avg.)	.086	.024
Saturation μ (cm^2 / V·s) (max.)	.157	.089
Saturation μ (cm^2 / V·s) (avg.)	.073	.031
On/Off (max.)	$1x10^5$	$4x10^4$
On/Off (avg.)	$4.5x10^4$	$2.5x10^4$
On Current (max.)	$1.8x10^{-5}$	$5.6x10^{-6}$
On Current (avg.)	$9.6x10^{-6}$	$2.1x10^{-6}$
Threshold Voltage (min.)	10	30
Threshold Voltage (avg.)	21	36

Table 1: Maximum and average of OFET transfer and output characteristics

CHAPTER 5: CONCLUSION AND FUTURE WORK SUGGESTION

5.1 Summary

To summarize, we have fabricated an n-type organic field effect transistor using aligned arrayed carbon nanotube electrodes. These densely aligned CNT arrays were assembled by DEP, which is a simple process possible in room temperature and atmospheric conditions. In order to create the actual CNT electrodes, we used EBL and oxygen plasma to create a 2μm channel length. By the method of thermal evaporation we deposited a layer of C60 polymer as the semiconducting material for the OFET and performed measurements inside a nitrogen-rich glove-box. As our control device we fabricated gold electrode OFETs with the same dimension as our CNT electrode OFETs.

When analyzing the electron transport characteristics we obtained a higher maximum and average on-current, mobility, and on/off ratio in the CNT electrodes OFETs compared to the control gold electrode OFETs. In addition, we also observed a lower minimum and average threshold voltage in OFETs made with CNT electrodes. Consequently we can conclude that this better charge injection showed in CNT OFETs shows are a better charge injection electrode due to the strong π-π interaction between the CNT electrode and the organic material interface. Another attribute that leads to a better charge injection is the one-dimensional, open-ended tubes that the CNT electrode possesses.

Fabricating n-type OFETs implementing CNT electrodes leads to a better charge injection, thus a method to fabricate n-type OFETs for applications such as logic circuits was reported in this thesis.

5.2 Future work suggestions

The result of this work can be used for other research areas to improve the contact resistance and charge injection of OFETs using aligned array carbon nanotube electrodes. Our group does low-temperature measurements, so this project has potential to be analyzed in low-temperature measurements. This will give us a better understanding of the activation energy of the C60 (n-type) OFET. Besides researching the activation energies we can measure contact resistance at low temperature. This will give us a numerical value for the actual resistance presence between the CNT and organic semiconductor interface. In addition, we can also measure the barrier height and width at the CNT/organic interface.

Another potential future plan could be fabricating n-type OFETs with a smaller channel length. With this we can study these n-type OFETs behaviors at short channel lengths.

CHAPTER 6: REFERENCES

1. Braga, D. and G. Horowitz, *High-Performance Organic Field-Effect Transistors.* Advanced Materials, 2009. **21**(14-15): p. 1473-1486.
2. Avouris, P. and R. Martel, *Progress in carbon nanotube electronics and photonics.* MRS Bulletin, 2010. **35**(04): p. 306-313.
3. Aguirre, C.M., et al., *Carbon Nanotubes as Injection Electrodes for Organic Thin Film Transistors.* Nano Letters, 2009. **9**(4): p. 1457-1461.
4. Tiwari, S.P., et al., *Solution-Processed n-Type Organic Field-Effect Transistors With High ON /OFF Current Ratios Based on Fullerene Derivatives.* Electron Device Letters, IEEE, 2007. **28**(10): p. 880-883.
5. Zaumseil, J. and H. Sirringhaus, *Electron and Ambipolar Transport in Organic Field-Effect Transistors.* Chemical Reviews, 2007. **107**(4): p. 1296-1323.
6. Liu, J. and M.C. Hersam, *Recent developments in carbon nanotube sorting and selective growth.* MRS Bulletin, 2010. **35**(04): p. 315-321.
7. Cicoira, F., C.M. Aguirre, and R. Martel, *Making Contacts to n-Type Organic Transistors Using Carbon Nanotube Arrays.* ACS Nano, 2010. **5**(1): p. 283-290.
8. Sarker, B.K., et al., *Fabrication of Organic Field Effect Transistor by Directly Grown Poly(3 Hexylthiophene) Crystalline Nanowires on Carbon Nanotube Aligned Array Electrode.* ACS Applied Materials & Interfaces, 2011. **3**(4): p. 1180-1185.

9. Sarker, B.K. and S.I. Khondaker, *High-performance short channel organic transistors using densely aligned carbon nanotube array electrodes.* Applied Physics Letters, 2012. **100**(2): p. 023301-4.

10. *Transparent*. Available from: http://www.onlyoled.co.uk/korean-researchers-develop-transparent-transistors-oled-displays.

11. *Flexible*. Available from: http://www.smartertechnology.com/c/a/Technology-For-Change/3-Reasons-Flexible-Electronics-Enable-Smarter-Displays-/.

12. Hill, I.G., et al., *Molecular level alignment at organic semiconductor-metal interfaces.* Applied Physics Letters, 1998. **73**(5): p. 662-664.

13. Koch, N., et al., *Conjugated organic molecules on metal versus polymer electrodes: Demonstration of a key energy level alignment mechanism.* Applied Physics Letters, 2003. **82**(1): p. 70.

14. Lee, M.H.J. and R.J. Collier, *Sheet resistance measurement of thin metallic films and stripes at both 130 GHz and DC.* Instrumentation and Measurement, IEEE Transactions on, 2005. **54**(6): p. 2412-2415.

15. Stokes, P. and S.I. Khondaker, *Local-gated single-walled carbon nanotube field effect transistors assembled by AC dielectrophoresis.* Nanotechnology, 2008. **19**(17): p. 175202.

16. Di, C.-a., et al., *Interface Engineering: An Effective Approach toward High-Performance Organic Field-Effect Transistors.* Accounts of Chemical Research, 2009. **42**(10): p. 1573-1583.

17. Jung, B.J., et al., *Molecular Design and Synthetic Approaches to Electron-Transporting Organic Transistor Semiconductors†.* Chemistry of Materials, 2010. **23**(3): p. 568-582.

18. Chua, L.-L., et al., *General observation of n-type field-effect behaviour in organic semiconductors.* Nature, 2005. **434**(7030): p. 194-199.

19. Dimitrakopoulos, C.D. and P.R.L. Malenfant, *Organic Thin Film Transistors for Large Area Electronics.* Advanced Materials, 2002. **14**(2): p. 99-117.

20. de Leeuw, D.M., et al., *Stability of n-type doped conducting polymers and consequences for polymeric microelectronic devices.* Synthetic Metals, 1997. **87**(1): p. 53-59.

21. Seo, J.H., et al., *Improved Injection in n-Type Organic Transistors with Conjugated Polyelectrolytes.* Journal of the American Chemical Society, 2009. **131**(51): p. 18220-18221.

22. Wobkenberg, P.H., et al., *Fluorine containing C[sub 60] derivatives for high-performance electron transporting field-effect transistors and integrated circuits.* Applied Physics Letters, 2008. **92**(14): p. 143310-3.

23. Schroeder, R., L.A. Majewski, and M. Grell, *Improving organic transistor performance with Schottky contacts.* Applied Physics Letters, 2004. **84**(6): p. 1004-1006.

24. Wang, S.D., et al., *Contact-metal dependent current injection in pentacene thin-film transistors.* Applied Physics Letters, 2007. **91**(20): p. 203508.

25. Braun, S., W.R. Salaneck, and M. Fahlman, *Energy-Level Alignment at Organic/Metal and Organic/Organic Interfaces.* Advanced Materials, 2009. **21**(14-15): p. 1450-1472.

26. Shekhar, S., P. Stokes, and S.I. Khondaker, *Ultrahigh Density Alignment of Carbon Nanotube Arrays by Dielectrophoresis.* ACS Nano, 2011. **5**(3): p. 1739-1746.

27. Bürgi, L., et al., *Close look at charge carrier injection in polymer field-effect transistors.* Journal of Applied Physics, 2003. **94**(9): p. 6129.

28. Hamadani, B.H. and D. Natelson, *Extracting Contact Effects in Organic FETs.* Proceedings of the IEEE, 2005. **93**(7): p. 1306-1311.

29. Klauk, H., et al., *Contact resistance in organic thin film transistors.* Solid-State Electronics, 2003. **47**(2): p. 297-301.

30. McEuen, P.L., *Single-wall carbon nanotubes.* Physics World, 2000. **13**(6): p. 31-36.

31. Jha, A. *Carbon nanotubes may suppress human immunity*. 2009 [cited 2012 April 19]; Available from: http://www.guardian.co.uk/science/2009/jun/15/carbon-nanotubes-immune-system-nanotechnology.

32. Guo, X. and C. Nuckolls, *Functional single-molecule devices based on SWNTs as point contacts.* Journal of Materials Chemistry, 2009. **19**(31): p. 5470-5473.

33. Qi, P., et al., *Miniature organic transistors with carbon nanotubes as quasi-one-dimensional electrodes.* Journal of the American Chemical Society, 2004. **126**(38): p. 11774-11775.

34. Guo, X., et al., *Photoresponsive nanoscale columnar transistors.* Proceedings of the National Academy of Sciences, 2009. **106**(3): p. 691.

35. Sarker, B.K., et al., *Fabrication of Aligned Carbon Nanotube Array Electrodes for Organic Electronic Devices.* Materials Express, 2011. **1**(1): p. 80-85.

36. Southard, A., et al., *Solution-processed single walled carbon nanotube electrodes for organic thin-film transistors.* Organic Electronics, 2009. **10**(8): p. 1556-1561.

37. Hellstrom, S.L., et al., *Driving High-Performance n- and p-type Organic Transistors with Carbon Nanotube/Conjugated Polymer Composite Electrodes Patterned Directly from Solution.* Advanced Materials, 2010. **22**(37): p. 4204-4208.

38. Zhang, Y.Y., et al., *Poly(3,3'''-didodecylquarterthiophene) field effect transistors with single-walled carbon nanotube based source and drain electrodes.* Applied Physics Letters, 2007. **91**(22): p. 223512-223512-3.

39. Lee, C.W., et al., *Solution-Processable Carbon Nanotubes for Semiconducting Thin-Film Transistor Devices.* Advanced Materials, 2010. **22**(11): p. 1278-1282.

40. Li, J., et al., *Fabrication of carbon nanotube field effect transistors by AC dielectrophoresis method.* Carbon, 2004. **42**(11): p. 2263-2267.

41. Kent, P. *The C60 "buckyball" fullerene*. 2004; Available from: http://www.ornl.gov/~pk7/pictures/c60.html.

42. Zhang, X.H., B. Domercq, and B. Kippelen, *High-performance and electrically stable C60 organic field-effect transistors.* Applied Physics Letters, 2007. **91**(9): p. 092114.

43. Rinzler, A., et al., *Unraveling nanotubes: field emission from an atomic wire.* Science, 1995. **269**(5230): p. 1550-1553.